ARCHIVES OF ACOUSTICS
17, 3, 389–412 (1992)

SURFACE ACOUSTIC WAVE SCATTERING BY ELLIPTIC METAL DISK ON ANISOTROPIC PIEZOELECTRIC HALFSPACE

E. DANICKI

Institute of Fundamental Technological Research
Polish Academy of Sciences
(00-049 Warszawa, Świętokrzyska 21)

Surface acoustic wave (SAW) propagating in arbitrarily anisotropic piezoelectric halfspace is considered. The wave interacts with a perfectly conducting and weightless metal disk on the substrate surface by means of the electric potential only which is coupled to SAW due to the substrate piezoelectricity. A perturbation theory of scattering plane harmonic SAW by the disk is presented which accounts the dielectric, and elastic anisotropy of the substrate. The solution for electric charge distribution on the disk is given in a form of fast convergent series easy for computation. The total electric charge induced by SAW on the grounded disk is explicitly evaluated. Angular dependences of the scattered SAW in large distance from the disk is also discussed.

1. Introduction

Surface acoustic wave propagating in a piezoelectric halfspace is accompanied with a wave of electric potential on the halfspace surface. Perturbation of the potential allows scattering SAW. This phenomenon is exploited for some technical purposes in SAW devices. The theory presented below concerns SAW scattering by perfectly conducting elliptic disk on anisotropic piezoelectric substrate.

There are similar problems in acoustics and electromagnetics, where a rigorous theory has been developed of wave scattering by ellipsoid and, in limit, by disk [1]. Perturbation theories are also known for small disks [2], [3]. The problem considered in this paper differs from the above ones at least with the substrate anisotropy. The dielectric anisotropy of the substrate directly effects the electric charge distribution on the disk induced by the incident SAW. This, and the angular dependence of SAW velocity and SAW coupling to the electric field resulting from the elastic and piezoelectric anisotropy of the substrate, influence on the angular dependence of the scattered SAW far-field.

The theory presented below is a perturbation one. It relys on neglecting of piezoelectric interaction when the electric charge distribution on the disk is evaluated. This simplification can be applied under the assumption of weak piezoelectricity of the substrate or on the assumption that the disk diameter is not excessively large as compared to the wavelength of SAW.

The formulation of the boundary problem considered is given in Section 2. Appendix B shows how the problem for elliptic disk can be transformed into the problem for circular disk of unit radius. The transformation results however in anisotropic Green's function, which is discussed in Appendix A. Section 3 presents the solution of certain electrostatic problem for anisotropic dielectric halfspace (much more elegant solution was recently presented in [18]). The key features of this solution are discussed in Appendix C. Section 4 is devoted to the evaluation of electric charge distribution induced on the disk by the incident SAW. The scattered SAW is considered in Section 5 where some numerical examples are also presented.

Note. In the paper, several functions are represented in a form of infinite or finite series which components, as well as summation limits are described separately in the main text or in Appendices. To clarify the presentation of the formulas the symbols of summation are usually dropt (there are notes about it however from time to time).

2. Integral formulation of the scattering problem

2.1. Simplified description of the substrate electric property

Consider a traction-free piezoelectric substrate surface with electric charge distribution in a form of the travelling wave on it

$$\Delta D_{\perp} = \rho \exp(j\omega t - j\mathbf{k} \cdot \mathbf{r}) \tag{1}$$

where the denotation $\Delta D_{\perp}$ expresses well known relation between surface electric charge and the discontinuity of electric flux density on both sides of the surface [4], ω – angular frequency (in what follows, the time dependence will be droped), $\mathbf{k}$ – wave-vector, ρ – complex amplitude of the surface electric charge.

Following [5], [6] the wave of electric charge results in the wave of electric potential on the substrate surface. The potential complex amplitude is

$$\Phi = G(\omega, \mathbf{k})\rho \tag{2}$$

where G is the Fourier transform of electric Green's function of the piezoelectric halfspace (the considered Green's function concerns the electric quantities on the halfspace surface only).

Generally, G can be decomposed into three components describing three different physical phenomena, dielectric property of the substrate, generation of surface acoustic wave or bulk acoustic waves coupled to the surface electric potential. A detailed discussion of the function G is given elsewhere [7], [8], let us only note here that both two

former components are singular functions of wave-number k, while the latter component is usually bounded function of k.

In what follows, the latter part of G describing bulk waves is completely neglected, however there are not any substantial difficulties in including it into considerations on a similar way as the surface waves.

Following this simplification we have

$$G(\mathbf{k}) = \frac{1}{k\varepsilon_e}\frac{k^2 - k_0^2}{k^2 - k_v^2} \tag{3}$$

where $k = \|\mathbf{k}\|$, and k_0 – wave-number of SAW for metalized substrate surface, k_v – wave-number of SAW for free substrate surface, ε_e – effective surface permittivity of the substrate, all the above quantities depend on the direction of propagation of the wave $\mathbf{k}/k$, note however that due to point symmetry there is $\varepsilon_e(\vartheta + \pi) = \varepsilon_e(\vartheta)$ and similarly for k_0 and k_v.

It is convenient to write the relation (2) in spatial representation as follows

$$\Phi(\mathbf{r}) = \iint_S g(\mathbf{r}; \mathbf{r}')\rho(\mathbf{r}')dS' \tag{4}$$

where the integral is taken over the whole surface occupied by the electric charge. Explicit form of g is given in Appendix A.

2.2. Simplified formulation of the scattering problem

It is shown in Appendix B how the problem for elliptic disk can be led to the problem for circular one. It is done by suitable scaling and subsequent transformation of the coordinate system. The following considerations concern the transformed spatial coordinates where we have to do with circular disk of unit radius.

Let us consider the grounded disk which electric potential is zero. With help of (4) this can be expressed in a form

$$-\Phi^0(\mathbf{r}) = \iint_S g(\mathbf{r}; \mathbf{r}')\rho(\mathbf{r}')dS' \tag{5}$$

where $\mathbf{r}$ and $\mathbf{r}'$ belong to the disk area S where $\|\mathbf{r}\| \le 1$, and Φ^0 is the incident wave potential on the free substrate surface

$$\Phi^0 = \exp(jk_v z) \tag{6}$$

(for convenience, we apply the unitary potential amplitude and incident SAW propagating in $-z$-axis direction).

In the case of free (floating) disk where the disk potential can have nonzero value (constant over the whole disk), the scattering problem can be divided into three parts which can be solved separately.

i) firstly, the solution for grounded disk should be found and the total electric charge Q induced on the disk evaluated,

ii) secondly, an auxiliary problem should be solved for grounded disk with $-\Phi^0 = V = \text{const}$ applied instead of (6). The total electric charge Q_0 over the disk should be evaluated in this case, too,

iii) the last step is to make a superposition of both solutions with V chosen in such a way that $Q + Q_0 = 0$. The potential V is the floating disk potential induced by the incident SAW.

The problem ii) describes also the generation of SAW by a disk supplied with an external voltage, it can be solved on a similar way as the problem i).

The integral equation (5) is very complicated and, generally, it can not be solved exactly. However, for common piezoelectric substrates we can apply the assumption of weak piezoelectric coupling, that is

$$\Delta v/v = (k_0 - k_v)/k_v << 1 \tag{7}$$

This enable us to apply the iteration procedure in solving (5), speaking in advance we will perform only first step of the iteration.

Applying results given in Appendix A we can write

$$-\Phi^0 = \iint_S g^E \rho \, dS + \iint_S g^R \rho \, dS \tag{8}$$

where g^E is a singular function at $\mathbf{r} = \mathbf{r}'$, while g^R is a regular function proportional to $\Delta v/v$ which value is relatively small. It means that the second component in (8) can be neglected for all $\mathbf{r}$ in vicinity of $\mathbf{r}'$, say for all $\mathbf{r}$ from the disk area S.

Following this simplification the first approximation to (8) is

$$-\sum_m J_m(kr) e^{jm\vartheta} = \iint_S \frac{\rho(r', \vartheta')}{2\pi \bar{r} \varepsilon_e(\bar{\vartheta} - \pi/2)} dx' dy' =$$

$$\frac{1}{2\pi} \int_0^{2\pi} [\, \varepsilon_e(\bar{\vartheta} - \pi/2) \,]^{-1} d\bar{\vartheta} \int_0^{R(\bar{\vartheta})} \rho(r', \vartheta') \, d\bar{r} \tag{9}$$

where $\bar{r} = \|\mathbf{r} - \mathbf{r}'\|$, $\bar{\vartheta} = \arg\{(\mathbf{r} - \mathbf{r}')/\bar{r}\}$ similarly r, ϑ and r', ϑ' represent vectors $\mathbf{r}$ and $\mathbf{r}'$ in polar coordinates on the substrate surface (Fig. 1). The left-hand side of (9) is $-\Phi^0$ in polar coordinates r, ϑ. The equation (9) is the weekly singular Fredholm integral equation of the first kind for charge distribution ρ.

Confining our consideration to the first approximation, the far-field solution for the scattered SAW can be evaluated with help of asymptotic representation for g^R (see Appendix A), that is

$$\Phi(r \to \infty, \vartheta) = \iint_S g^A(\vartheta; r', \vartheta') \rho(r', \vartheta') \, dS' \tag{10}$$

where ρ is the solution of (9).

3. An auxiliary electrostatic problem

3.1. Arbitrary distribution of electric charge over the disk

Charge distribution which is a smooth function over the circular disk can be represented by a series (summation over m, n will not be explicitly marked troughout the paper)

$$\rho(r', \vartheta') = \sigma_{mn} \frac{T_n(r')}{(1 - r'^2)^{1/2}} e^{jm\vartheta'} \tag{11}$$

where T_n is the n–th order Tchebyshev polynomial and σ_{mn} is an arbitrary constant. The applied charge distribution (11) exhibits square-root singularity at $r' \to 1$ which is typical for the problem considered here [2]. The condition that $\rho(r', \vartheta') \equiv \rho(-r', \vartheta' + \pi)$ constrains n in (11) to numbers having the same parity as m.

Substitution of the above representation into (9) gives the potential Φ under the disk (that is for $r \leq 1$) in the form (see Fig. 1 for geometric interpretation of r_1 and r_2)

$$\phi = \frac{1}{4\pi} \int_0^{2\pi} d\bar{\vartheta} \chi(\bar{\vartheta} - \pi/2) \int_{-(1-r_1^2)^{1/2}}^{(1-r_1^2)^{1/2}} \rho(r', \vartheta') dr_2 \tag{12}$$

where $\chi = 1/\varepsilon_e$ and

$$\begin{aligned} r_1 &= r \sin(\bar{\vartheta} - \vartheta) \\ r_2 &= \bar{r} + r \cos(\bar{\vartheta} - \vartheta) \\ r' &= (r_2^2 + r_1^2)^{1/2} \\ \vartheta' &= \bar{\vartheta} - \frac{1}{2} \arg[\,(-r_2 + jr_1)/(-r_2 - jr_1)\,] \end{aligned} \tag{13}$$

where $\arg\{e^{j\alpha}\} = \alpha$.

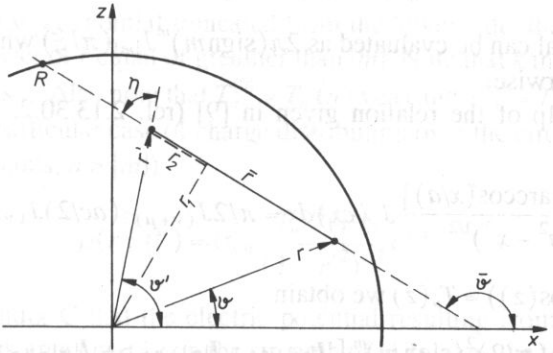

FIG. 1. Geometrical interpretation of integral variables.

It follows from (13) that the substitution can be made

$$r_1 = \xi \sin\eta$$
$$r_2 = \xi \cos\eta \tag{14}$$

resulting in variables

$$\vartheta' = \bar{\vartheta} - \eta$$
$$r' = \xi \tag{15}$$

both dependent on r_2 and $\bar{\vartheta}$, which applied to (12) yield

$$\phi = \frac{\sigma_{mn}}{4\pi} \int_0^{2\pi} \chi(\bar{\vartheta} - \pi/2) e^{jm\bar{\vartheta}} d\bar{\vartheta} \int_{-(1-r_1^2)^{1/2}}^{(1-r_1^2)^{1/2}} \frac{T_n(\xi)}{(1-\xi^2)^{1/2}} e^{-jm\eta} dr_2 \tag{16}$$

Let us introduce an auxiliary function $f(r_1)$ the domain of which is $-1 \le r_1 \le 1$ so that $f(r_1)$ can be further expanded into a Fourier series as follows

$$f(r_1) = \int_{-(1-r_1^2)^{1/2}}^{(1-r_1^2)^{1/2}} \frac{T_n[(r_1^2 + r_2^2)^{1/2}]}{(1 - r_1^2 - r_2^2)^{1/2}} e^{-jm\eta} dr_2 = \sum_{l=-\infty}^{\infty} c_l e^{-j\pi l r_1} \tag{17}$$

where

$$c_l = \frac{1}{2} \int_{-1}^{1} dr_1 e^{j\pi l r_1} \int_{-(1-r_1^2)^{1/2}}^{(1-r_1^2)^{1/2}} \frac{T_n[(r_1^2 + r_2^2)^{1/2}]}{(1 - r_1^2 - r_2^2)^{1/2}} e^{-jm\eta} dr_2 \tag{18}$$

We easily note that the integration area in the double integral (18) appears to be a circle of unitary radius on the plane (r_1, r_2) then applying new polar coordinates (14) the integral (18) can be transformmed into

$$c_l = \frac{1}{2} \int_0^1 \frac{\xi T_n(\xi)}{(1-\xi^2)^{1/2}} d\xi \int_0^{2\pi} e^{j\pi l \xi \sin\eta} e^{-jm\eta} d\eta \tag{19}$$

The second integral can be evaluated as $2\pi(\operatorname{sign} m)^m J_{|m|}(\pi l \xi)$ where $\operatorname{sign}\{m\} = +1$ for $m \ge 0$ and -1 otherwise.

Now, with help of the relation given in [9] (rel. 2.13.30.2, p.209) for $a > 0$ and $\nu > -1$

$$\int_0^a \frac{\cos[\mu \arccos(x/a)]}{(a^2 - x^2)^{1/2}} J_\nu(cx) dx = \pi/2 J_{(\nu+\mu)/2}(ac/2) J_{(\nu-\mu)/2}(ac/2)$$

where $\cos(n \arccos(z)) = T_n(z)$ we obtain

$$c_l^{(m,n)} = (\pi/2)^2 (\operatorname{sign} m)^m \left[J_{\frac{|m|-n+1}{2}} J_{\frac{|m|+n-1}{2}} + J_{\frac{|m|-n-1}{2}} J_{\frac{|m|+n+1}{2}} \right] \tag{20}$$

where the argument of each Bessel function J above is $\pi l/2$. Also note that all these Bessel functions have half-integer indices because m and n have the same parity. Upper indices in the left-hand side of (20) mark the dependence of c_l on m and n.

It is easy to prove that

$$c_0^{(m,n)} = 0, \quad \text{for } m \neq 0 \text{ and arbitrary } n,$$

$$c_0^{(0,n)} = \pi(-1)^{n/2}(1-n^2)^{-1}, \quad \text{for } m = 0 \ (n \text{ even}). \tag{21}$$

Some further properties of the coefficients c are discussed in Appendix C.

Having $f(r_1)$ expanded into the Fourier series (17) the relation (16) gives after simple transformation

$$\phi = \frac{1}{2}\sigma_{kn}\chi_{m-k}c_l^{(k,n)}e^{jm\vartheta}J_m(\pi l r) \tag{22}$$

(note that there are summations over m, k and l in infinite limits and after n from 0 to ∞). Taking into account (C.2) the above relation can be further transformed into

$$\Phi = \frac{1}{2}\sigma_{kn}\chi_{m-k}e^{jm\vartheta}J_m(\pi l r)\begin{cases}\left[\dfrac{a_p^{(k,n)}}{(\pi l)^p}(-1)^l + \dfrac{b_p^{(k,n)}}{(\pi l)^p}\right] & \text{for } l \neq 0 \\ c_0^{(k,n)} & \text{for } l = 0\end{cases} \tag{23}$$

(summation after p – see Appendix C).

3.2. *Particular case of charge distribution*

Let us introduce a polynomial (m and n have the same parity, $n \geq 0$)

$$T_n^{(m)}(r) = \sum_{k=|m|(2)}^{n} w_k r^k, \quad |m| \leq n \tag{24}$$

which is a Tchebyshev polynomial truncated from the lower side, the only components left are these with power of r equal or greather than $|m|$. Note that k in the definition (24) has the same parity as n. Also note that $T_n^{(0)} = T_n$ (n even) and $T_n^{(1)} = T_n$ (n odd).

Consider now a particular case of charge distribution over the circular disk in a form (σ_{mn} – arbitrary constants, $n \geq |m|$)

$$\rho(r', \vartheta') = \sigma_{mn}\frac{T_n^{(m)}(r')}{(1-r'^2)^{1/2}}e^{jm\vartheta'} \tag{25}$$

It is shown in Appendix C that the electric potential resulting from the above charge distribution in the disk area ($r < 1$) on the strength of (12) takes the form similar to (23) but without terms $(+1)^l/l^p$, that is (summation over m, n, l and p as previously)

$$\Phi = \frac{1}{2}\sigma_{kn}\chi_{m-k}e^{jm\vartheta}\cdot \begin{cases} 0; & \text{for } l=0 \text{ and } m\neq 0 \\ (-1)^l \dfrac{\alpha_p^{(k,n)}}{(\pi l)^p} J_m(\pi l r); & \text{for } l\neq 0 \\ c_0^{(0,n)}; & \text{for } l=0 \text{ and } k=0 \end{cases} \tag{26}$$

where $\alpha_p^{(k,n)}$ can be expressed by $a_p^{(k,n)}$ by suitable superposition (C.5) (transforming (23) to (26) we took into account that $J_m(0)=0$ for $m\neq 0$ as well as (21) and Appendix C).

Moreover, some components in (26) can be completely neglected because ([9], rel. 5.7.19.9, p.678)

$$\sum_{k=1}^{\infty}(-1)^k k^{2n-\nu}J_\nu(kx)=0 \;;\; 0<x<\pi \;,\; \nu-2n>1/2$$

It means that all components with $p<|m|$ in (26) can be dropt independently on the values of σ_{kn} and $\alpha_p^{(k,n)}$.

Let us consider net, or total electric charge on the disk resulting from integration of charge distribution (25) over the whole disk. We have (summation after even n)

$$Q=\iint_S \rho dS = 2\pi\sigma_{0n}\int_0^1 \frac{rT_n(r)}{(1-r^2)^{1/2}}dr = 2\pi\sigma_{0n}\frac{(-1)^{n/2}}{1-n^2} = 2c_0^{(0,n)}\sigma_{0n} \tag{27}$$

4. Charge distribution induced by SAW

4.1. Approximation of the incident potential wave

In (9) the wave of electric potential coupled to incident SAW is represented in polar coordinates. This representation can be further expanded with help of the relations given in [9], rel. 5.7.17. (26) and (2) (below taken with $n=1$)

$$\sum_{k=1}^{\infty}(-1)^{k+1}\frac{k^{2n-\nu}}{k^2-a^2}J_\nu(kx)=\frac{\pi}{2}a^{2n-\nu-1}\operatorname{cosec}(a\pi)J_\nu(ax)$$

$$\sum_{k=0}^{\infty}(-1)^k J_0(kx)=\frac{1}{2} \;;\; \nu>2n-5/2\,,\; n=1,2,\ldots\,,\; 0<x<\pi$$

The result is (summation over m dropt)

$$-\Phi^0 = -\frac{\sin k_v}{k_v}e^{jm\vartheta}\sum_{l=-\infty}^{\infty}(-1)^l\cdot \begin{cases} 0; & \text{for } l=0 \text{ and } m\neq 0 \\ \dfrac{(k_v/\pi l^{-|m|-\nu}}{1-(k_v/\pi l)^2}J_m(\pi l r); & l\neq 0 \\ 1; & \text{for } l=0 \text{ and } m=0 \end{cases} \tag{28}$$

where $\nu=2$ for $m=0$ and $\nu=0$ for $m\neq 0$.

As known, $J_m(\pi l r) \sim 1/\sqrt{l}$ for large l and $r \neq 0$. It means that the above series over l is absolutely convergent for all m and $0 < r < 1$ under consideration. Allowing certain error of an order of $O(1/N)$, components with large l, say with $|l| > N$ can be omited when the series is evaluated. Thus we can replace infinite limits of summation over l in (28) with $\pm N$, where $N >> k_v/\pi$.

Now consider Lagrange interpolation allowing representation of $[l^2 - (k_v/\pi)^2]^{-1}$ in a form of finite series of terms like l^{-2p}, $p = 1, 2, ..., N$ with strict equality of both representations for $|l| = 1, 2, ..., N$ (see Appendix D). Applying this representation in (28) we obtain series like

$$\sum_{l=1}^{N} (-1)^l \sum_{p=1}^{N} \frac{\beta'_p}{l^{2p}} \left(\frac{k_v}{\pi l} \right)^{|m|+\nu} J_m(\pi l r)$$

(ν as above in (28)). Once more it is seen that the summation over l can be extended to infinity with error of an order of $O(l/N)$.

Finally, an admissible approximation to (28) is

$$-\Phi^0 = -\frac{\sin k_v}{k_v} e^{jm\vartheta} \sum_{l=-\infty}^{\infty} (-1)^l \begin{cases} 0; & \text{for } l = 0 \text{ and } m = 0 \\ \sum_{p=\nu+|m|(2)}^{N} \frac{\beta_p^{(m)}}{(\pi l)^p} J_m(\pi l r); & l \neq 0 \\ l; & \text{for } l = 0 \text{ and } m = 0 \end{cases} \qquad (29)$$

where summation over m is limited to $|m| < M$ and β_p appearing above are corresponding coefficients of the Lagrange interpolation calculated for N dependent on $|m|$, namely for $N_m = N - |m|$. Note that p varies from $|m| + \nu$ to N by step of 2 so that both p and m have the same parity. To obtain good approximation one has to apply large value of N, at least to fulfil $N - M >> k_v/\pi$.

4.2. Evaluation of charge distribution

A comparison of (29) and (26) makes evident that:

i) electric charge distribution induced by SAW can be expanded into a series like (25), resulting in the similarity of both the above series.

ii) the expansion coefficients σ_{mn} can be evaluated on the strength of equality of similar components appearing in (26) and (29) at the same m and p.

iii) when comparing the above series, components with $p < |m|$ must be neglected what ensures that the number of equations equals the number of unknown (see Section 3.2).

A direct comparison of (29) and (28) takes place for every m and $p \neq 0$, and separately for free term at $l = 0$ (only for $m = 0$). On the strength of (21), (27) the later gives directly the total electric charge induced on the grounded disk by the incident wave of electric potential of unitary amplitude (6)

$$Q = (4/\chi_0) \frac{\sin k_v}{k_v} \qquad (30)$$

It follows from this relation taken for $k_v \to 0$ that the disk capacitance is [10], [15]

$$C = 4/\chi_0 \tag{31}$$

The simultaneous equations obtained as a result of the comparison ii) can be solved numerically on the usual way. However note that for the simplest case of circular disk on isotropic substrate, when only $\chi_0 \neq 0$ and the remaining $\chi_k = 0$ the simultaneous equations are separated for every m. What's more, the matrix of the equations has a triangular form in this case (this follows from the triangular form of truncated matrix $\alpha_p^{(\cdot,n)}$ for $p \geq |m|$, where the dot upper index means any particular value of m, see Appendix C and the discussion at the end of Section 3.2, below (26), concerning zero-valued series of Bessel functions).

It is seen that the above equations allow to evaluate all σ_{mn} except σ_{00} which can be evaluated on the strength of (30) and (27). This concludes the evaluation of charge distribution on a grounded disk. It was discussed in Section 2.2 above how it can be exploited in the case of free (floating) disk. The simple result is that the disk potential induced on the floating disk is $V = Q/C = \sin k_v / k_v$.

5. Angular dependence of the scattered far-field

5.1. Asymptotic analysis of the scattered SAW

Relation (10) describes the scattered electric potential wave on the substrate surface at point (r, ϑ), far from the disk, where the wave can be considered as plane wave which Poynting vector is oriented in direction ϑ. The double integral over the disk area S can be evaluated on the similar way as the integral (19) in Section 3 above. Indeed, we have after simple transformations with taking into account (C.2) (summation after m, n, k, note that g^A is inversely proportional to $\sqrt{r}$, see Appendix A)

$$\Phi = \iint_S g^A \rho \, dS' = \frac{C_\vartheta}{\sqrt{r}} \sigma_{mn} e^{jm(\theta_\vartheta + \pi/2)} \int_0^1 \frac{r'(T_n - t_k^{(m,n)} T_k)}{(1 - r'^2)^{1/2}} J_m(r' k_\vartheta) \, dr' \tag{34}$$

We easily note the similarity of every k-th term of (34) and (19), if only (πl) is replaced by k_ϑ. Thus we can write

$$\Phi = \frac{C_\vartheta}{\sqrt{r}} \sigma_{mn} e^{jm(\theta_\vartheta + \pi/2)} 2 \left(c_l^{(m,n)} - t_k^{(m,n)} c_l^{(m,k)} \right) \Big|_{(\pi l) = k_\vartheta} \tag{35}$$

Taking into account (C.2), (C.4) we see that

$$\Phi = \frac{C_\vartheta}{\sqrt{r}} \sigma_{mn} e^{jm(\theta_\vartheta + \pi/2)} \left[\frac{\alpha_p^{(m,n)}}{(\pi l)^p} \cos(\pi l) + \frac{\gamma_p^{(m,n)}}{(\pi l)^p} \sin(\pi l) \right] \Bigg|_{(\pi l) \to k_\vartheta \neq 0} \tag{36}$$

where α_p – see (C.5), similarly $\gamma_p = (\operatorname{sign} m)^m (d_p^{(m,n)} - \sum_m d_p^{(m,k)} t_k^{(m,n)})$.

Below we show that we need not evaluate all γ_p, but only γ_1 (for m even). Indeed, it is easy to prove that the right-hand side of (35) is a regular function at $k_\vartheta \to 0$, then (36) should be regular as well. It means, that every term like $\alpha\cos(k_\vartheta)/k_\vartheta$ must be accompanied with term like $\gamma\sin(k_\vartheta)/k_\vartheta^2$ just necessary to eliminate singularity from the expression $[\alpha\cos(k_\vartheta) + \gamma\sin(k_\vartheta)/k_\vartheta]/k_\vartheta$ at $k_\vartheta = 0$. This allows to evaluate γ for the given α.

Exactly, the expression in brackets in right-hand side of (36) can be rewritten as follows

$$\gamma_1 \sin k_\vartheta/k_\vartheta + \frac{\alpha_2\cos k_\vartheta + \gamma_3 \sin k_\vartheta/k_\vartheta + \dfrac{\alpha_4\cos k_\vartheta + \gamma_5 \sin k_\vartheta/k_\vartheta}{k_\vartheta^2} + \dots}{k_\vartheta^2}; \quad \text{for } m \text{ even}$$

$$\frac{\alpha_1\cos k_\vartheta + \gamma_2 \sin k_\vartheta/k_\vartheta + \dfrac{\alpha_3\cos k_\vartheta + \gamma_4 \sin k_\vartheta/k_\vartheta}{k_\vartheta^2} + \dots}{k_\vartheta}; \quad \text{for } m \text{ odd} \tag{37}$$

As we see, every γ_p can be evaluated from the given vector of α_p this way, except γ_1 which appears only for m even and which must be evaluated directly from (35), (36). It should be noted however that the above representation is not convenient for computation for small value of k_ϑ, in which case it is better to apply (35) and to evaluate suitable Bessel functions (20) in ordinary way.

5.2. Numerical examples

All results shown below (except Fig. 11) were obtained either for circular disk of unitary radius or for elliptic disk with main axes $1/\alpha$ and α (that is for $R = 1$, see Appendix B).

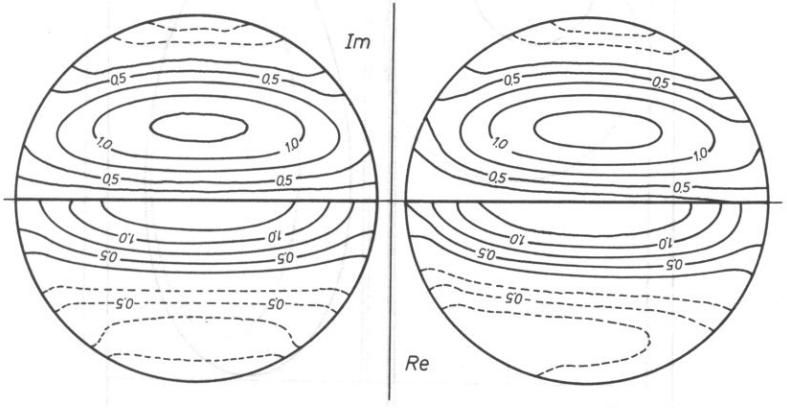

FIG. 2. Diagram of electric charge distribution on a circular disk of unitary radius for $k_v = \pi$. Left figure – isotropic substrate, right figure – dielectrically anisotropic substrate ($\chi_0 = 1$, $\chi_2 = -j.2$), upper part of the figures – imaginary component, and lower part – real component of $\rho(1 - r^2)^{1/2}$ (see relation (11)).

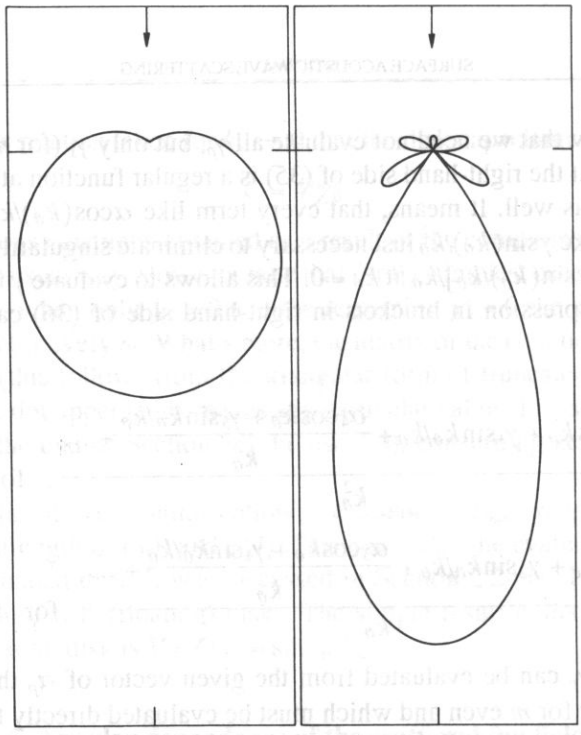

FIG. 3. Angular scattering pattern for grounded circular disk on isotropic substrate, $k_v = \pi/2$ (on left) and $k_v = 3\pi/2$ (right figure).

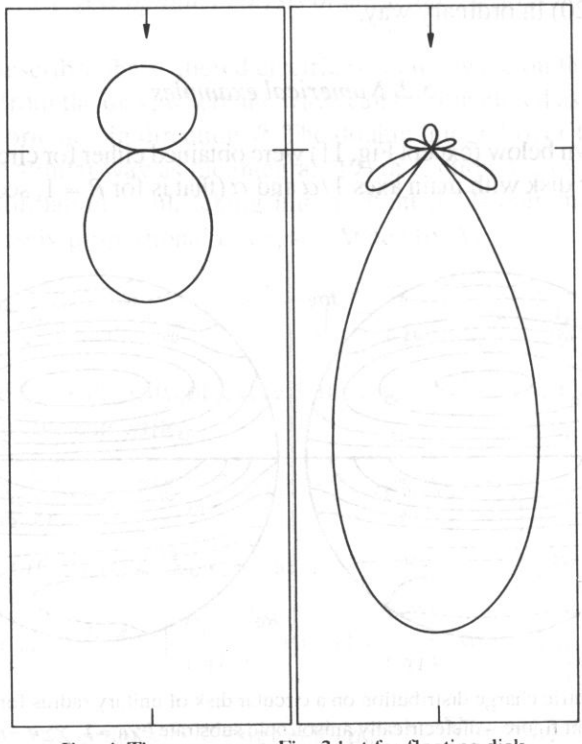

FIG. 4. The same as on Fig. 3 but for floating disk.

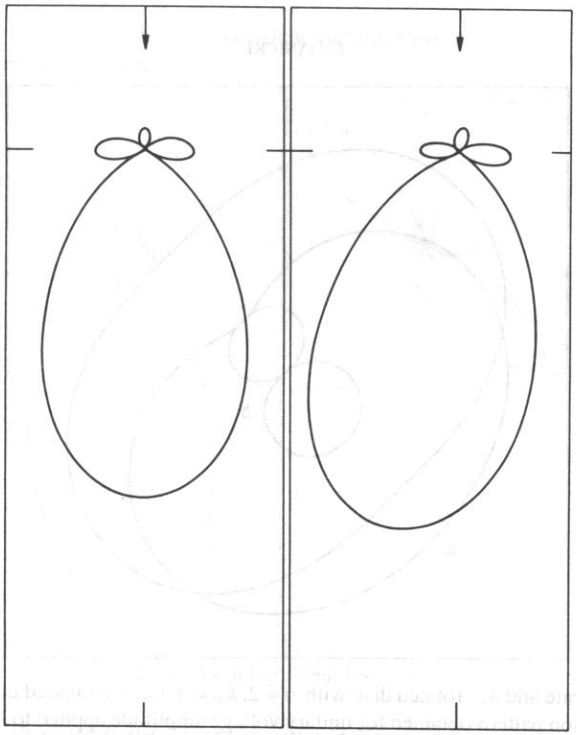

FIG. 5. Circular disk on isotropic (left) or anisotropic substrate (right, the dielectric anisotropy only, the same as in Fig. 2), for $k_v = \pi$.

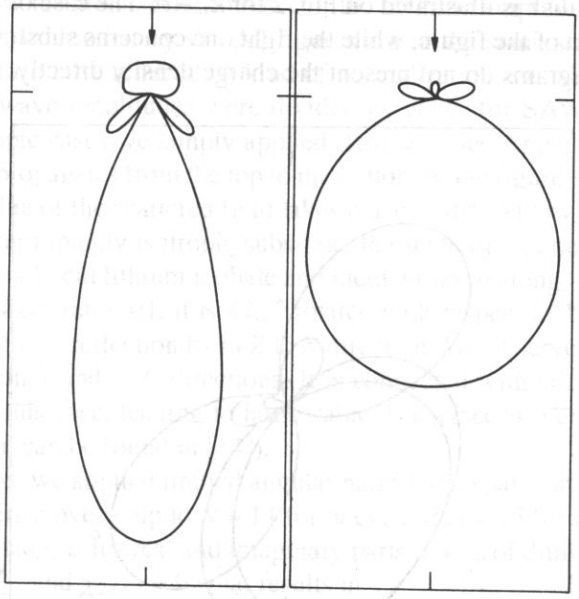

FIG. 6. Isotropic substrate and elliptic disk with $\alpha = \sqrt{2}$, longer axis horizontally oriented and $k_v = \pi\sqrt{2}$ (left figure), and vertically oriented and $k_v = \pi/\sqrt{2}$ (right figure), incident SAW from top of the figures.

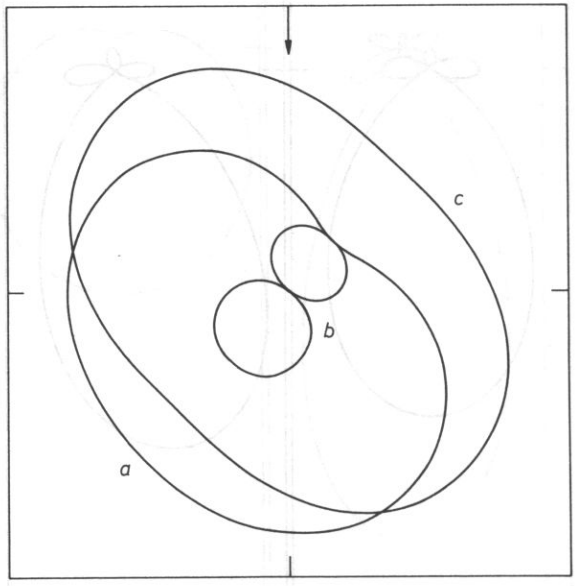

FIG. 7. Isotropic substrate and 45° rotated disk with $\alpha = 2$, $k_v = \pi/4$, a – grounded disk, b – floating disk, c – radiation pattern obtained for unitary voltage amplitude applied to the disk.

The influence of dielectric anisotropy of the substrate on the electric charge distribution on the circular disk is illustrated on Fig. 2 for $k_v = \pi$. The case of isotropic substrate is shown on left part of the figure, while the right one concerns substrate with $\chi_0 = 1$ and $\chi_2 = -j0.2$. The diagrams do not present the charge density directly, it illustrates rather

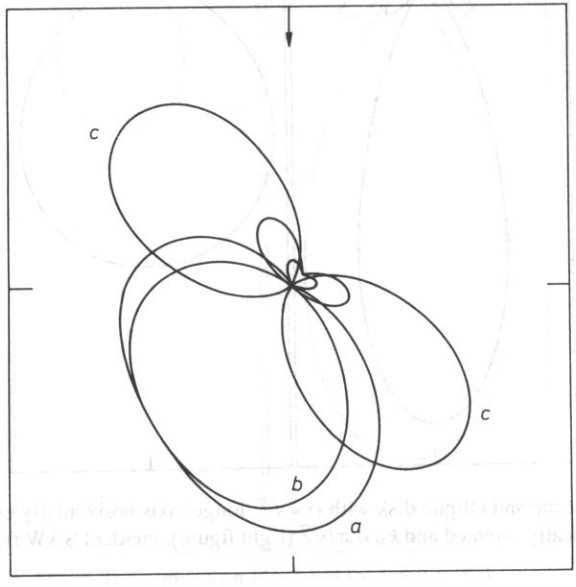

FIG. 8. As in Fig. 7 but for $k_v = \pi/2$.

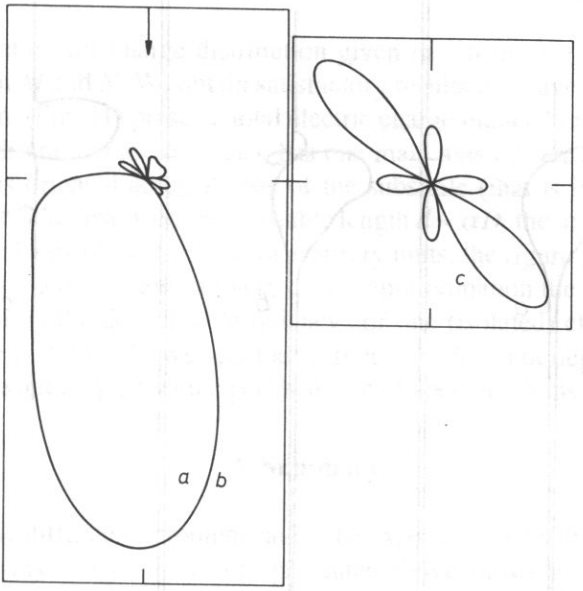

FIG. 9. As in Fig. 7 but for $k_v = \pi$.

the relation (25) with square-root term dropt for better presentation of the charge distribution in vicinity of the disk border. We see that the charge distribution is effected well by the dielectric anisotropy of the substrate.

Figs. 3–10 show the angular dependence of the far-field amplitude S (see (A.12)) of the scattered SAW, multiplied by $\sqrt{r}$. All figures are in the same scale except Fig. 10, which dimensions are 50% reduced. A kind of normalization was also applied, namely the values of the wave amplitudes were divided by $\Delta v/v$ for SAW propagating in z-direction (in isotropic cases we simply applied $\Delta v/v = 1$, see Appendix A). In all cases the incident wave propagates from the top to the bottom of the figures. As we see, in each case the largest value of the scattered field takes place in the shadow area.

Figs. 2–9 concern mainly isotropic substrate, the scattering patterns are rather typical. Fig. 10 concerns Y–cut lithium niobate and incident wave along $-Z$-axis. The disk is elliptic with main axes ratio 4:1, it is 47.2° rotated with respect to X-axis, as it is commonly applied for SAW reflection from Z to X direction. We observe large amplitude of the scattered field in + and − Z directions. It is connected with small curvature of the slowness curve in this case, leading to large value of C_ϑ (see Appendix A) for $\vartheta \approx 90°$ (detailed discussion can be found in [14]).

In computations, we applied limited angular harmonic expansion (25) with $|m|$ up to $M = 9$ and finite series over n up to $N = 14$ for m even or $N = 15$ for m odd. This results in simultaneous equations for real and imaginary parts of σ_{mn} of dimension up to 60*60. Note that $\chi_{-2n} = \chi^*_{2n}$ and $\chi_{2n+1} = 0$ what results in

$$\sigma_{-mn} = (-1)^m \sigma^*_{mn} \tag{38}$$

so that the equations are separated for even and odd m. The calculations can then be arranged in such a way that only components with $m \geq 0$ are to be evaluated. The conver-

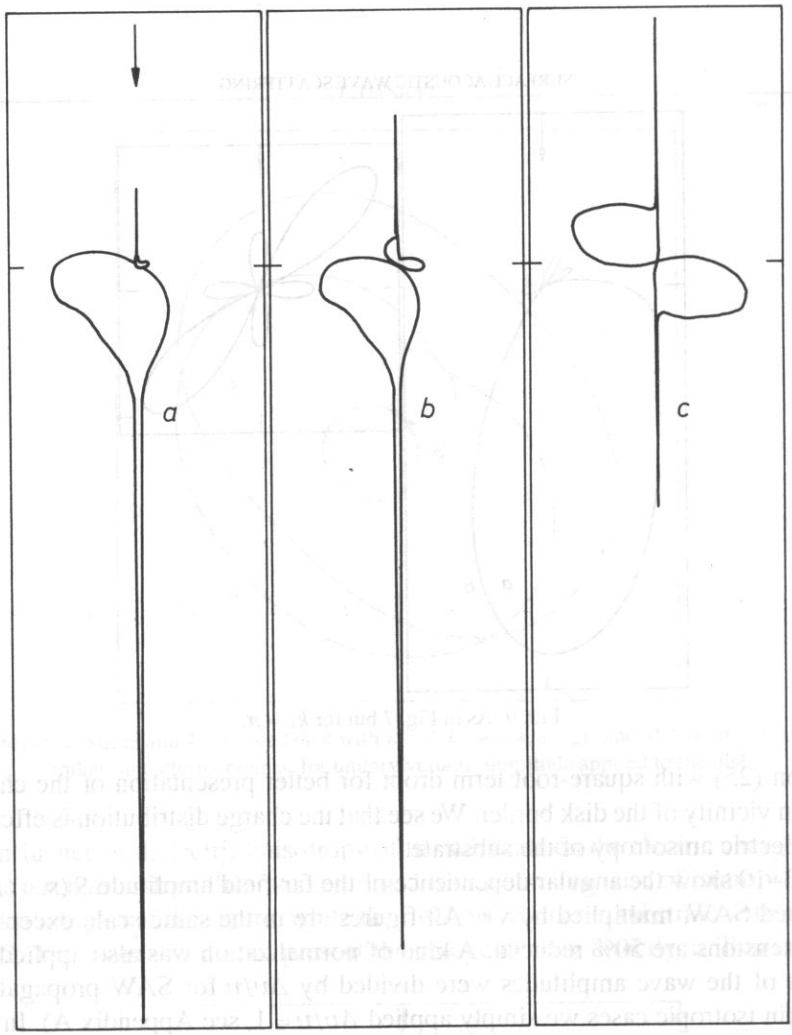

FIG. 10. 4:1 elliptic disk ($\alpha = 2$), 47.2° rotated with respect to X–axis of $LiNbO_3$, Y-cut, incident wave in $-Z$ direction (vertical axis of the figures), $k_v = \pi/2$, a, b, c – as in Fig. 7.

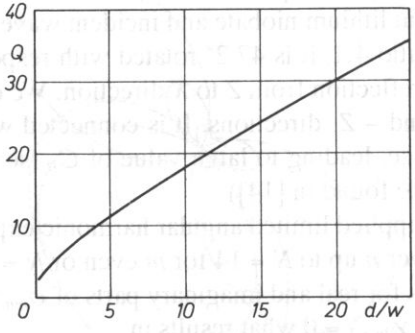

FIG. 11. The dependence of total electric charge amplitude Q induced on elliptic electrode on the electrode length d (that is on the disk main axis which is perpendicular to the direction of SAW propagation). Vertical axis in arbitrary units. The electrode width w is assumed constant, applied as a unit for figure horizontal axis.

gence of the solution for charge distribution given in a form of (25) was checked by applying different M and N. We obtain satisfactory results for wave-numbers up to 6.

The last figure (Fig. 11) presents total electric charge induced on the grounded elliptic disk on YZ lithium niobate. The disk has one main axis of constant (unitary) length $w = D/\alpha$ which is oriented along Z–axis of the substrate (that is in SAW propagation direction), and the other main axis has variable length $d = \alpha D$, the total charge is dependent on (the vertical axis of the figure is in arbitrary units, the figure presents the relation (30) with $k_v w$ assumed constant). In very coarse approximation the figure may be interpreted as concerning the detection "efficiency" of one (isolated) electrode of an interdigital transducer of SAW. As we see, the "efficiency" does not depend linearly on the electrode length what may effect the performance of apodized transducers [8].

6. Summary

An anisotropic diffraction problem cannot be expected to be solved explicitly so that computations are necessary. The theory presented above allows to perform some computations only once ($\alpha_p^{(m,n)}$ can be stored and applied in all cases). It is worth to note that important part of computations are performed with integer numbers (α_p are integer numbers), however the value of these numbers grows very fast with m, n, p, so that applying FORTRAN double precision variables on IBM-PC allows to perform exact computations with $|m| \le 9$ and $n \le 15$ only. This work was supported by grant 312129101.

Appendix A

With help of new spatial and spectral coordinates

$$k_x = k\cos\theta; \quad x = r\cos\vartheta$$
$$k_z = k\sin\theta; \quad z = r\sin\vartheta \tag{A. 1}$$

the inverse Fourier transform of $G(\mathbf{k})$ can be written as

$$g(r, \vartheta) = (2\pi)^{-2}\int_0^\infty dk \int_0^{2\pi} e^{-jrk\cos(\theta-\vartheta)}\chi(\theta)d\theta + \\ -(2\pi)^{-2}\int_0^\infty dk\int_0^{2\pi}\chi(\theta)\frac{k_0^2(\theta)-k_v^2(\theta)}{k^2-k_v^2(\theta)}e^{-jrk\cos(\theta-\vartheta)}d\theta \tag{A. 2}$$

where (n takes even values only because of polar symmetry of ε_e)

$$\chi(\theta) = 1/c_e(\theta) = \varepsilon_e(\theta+\pi) = \sum_{-\infty(2)}^{\infty}\chi_n e^{jn\theta} \tag{A. 3}$$

(2 in brackets means that n varies **step 2**).

First component of g is [11]

$$g^E(r, \vartheta) = \frac{1}{2\pi r}\chi(\vartheta+\pi/2) \tag{A. 4}$$

while the second one can be transformed into

$$g^R(r,\vartheta) = (2\pi)^{-1}\int_{-\infty}^{\infty} dk \int_0^{\pi} \frac{\Delta(\theta+\vartheta+\pi/2)}{k^2 - k_v^2(\theta+\vartheta+\pi/2)} e^{jrk\sin\theta} d\theta \tag{A. 5}$$

allowing to apply Jordan's lemma on the complex k–plane. The result is

$$g^R(r,\vartheta) = j/(4\pi)\int_{\vartheta-\pi/2}^{\vartheta+\pi/2} [\Delta(\theta')/k_v(\theta')] e^{-jrk_v(\theta')\cos(\theta'-\vartheta)} d\theta' \tag{A. 6}$$

where

$$\Delta/k_v = (k_0 + k_v)(k_0 - k_v)/(k_v\varepsilon_e) = 2(k_0 - k_v)/\varepsilon_e = 2\chi\Delta k$$

The function $g = g^E + g^A$ taken with arguments $(\bar{r}, \bar{\vartheta})$ describing vector $(\mathbf{r} - \mathbf{r}')$ in polar coordinates presents the electric Green's function for piezoelectric half-space. This function expresses electric potential at point $\mathbf{r}$ resulting from the point electric charge at point $\mathbf{r}'$, where both $\mathbf{r}$ and $\mathbf{r}'$ are on the substrate surface.

Let us evaluate the relation between $\|g^R\|$ and $\|g^E\|$ for the simplest case of isotropic substrate. We have

$$\|g^R\|/\|g^E\| < \pi r\,\Delta k \approx 20(\Delta v/v) r/\lambda$$

where $\Delta v/v$ is of an order of .001 for week piezoelectrics and .01 for strong ones ($\Delta v/v = .024$ for YZ lithium niobate). The above estimation means that in all cases g^R can be neglected when evaluating potential in the distance of about one wave-length λ from the point electric charge, and up to above 10λ for week piezoelectrics. This justifies the approximation (9) in the main text of the paper.

An asymptotic Green's function g for large value of r (it follows from the above reasoning that g^E can be neglected in this case) can be obtained applying the stationary phase method [12] to (A.6). Taking into account that

$$\bar{\mathbf{r}} = \mathbf{r} - \mathbf{r}' \tag{A. 8}$$

for $r \to \infty$, where r is the distance from the disk center to point (r, ϑ), where electric potential is evaluated, while (r', ϑ') is the point in the disk area, where electric charge is placed, and r is the distance between these two points, we obtain

$$g^A(\vartheta; r', \vartheta') = g^R(r \to \infty, \vartheta; r', \vartheta') \approx$$

$$\approx j/(2\pi)\int_{\vartheta-\pi/2}^{\vartheta+\pi/2} \chi(\theta')\Delta k(\theta') e^{-j(\mathbf{r}-\mathbf{r}')\cdot\mathbf{k}_v(\theta')} d\theta' \tag{A. 9}$$

Let us denote a stationary phase point as θ_ϑ (below we assume that there is only one such a point). This is an angle, for which the Poynting vector of the wave with wave-number $k_v(\theta_\vartheta)$ is directed to the observation point (r, ϑ) (as known, the Poynting vector is perpendicular to the slowness surface $k_v(\vartheta')$, here $\vartheta' = \theta_\vartheta$ [13]). The stationary phase method yields

$$\mathbf{k}'_\vartheta = \mathbf{k}_v(\theta_\vartheta) \tag{A. 10}$$

$$g^A(\vartheta; r', \vartheta') = \frac{C_\vartheta}{2\pi\sqrt{r}} \exp[jr' k_\vartheta \cos(\vartheta' - \theta_\vartheta)] e^{-j\mathbf{r}'\cdot\mathbf{k}_\vartheta} \qquad \text{(A. 10)}$$

[cont.]

$$C_\vartheta = \left[\frac{j2\pi}{\frac{d^2}{d\theta'^2}[k_v(\theta')\cos(\theta' - \vartheta)]\Big|_{\theta' = \theta_\vartheta}} \right]^{1/2} \chi(\theta_\vartheta)\Delta k_v(\theta_\vartheta)$$

on the assumption that the second derivative in the denominator in C_ϑ is different from zero [14]. Further transformations gives (phase term $\exp[-jrk_\vartheta\cos(\vartheta - \theta_\vartheta)]$ dropt)

$$g^A(\vartheta; r', \vartheta') = \frac{C_\vartheta}{2\pi\sqrt{r}} \sum_m J_m(r' k_\vartheta) e^{-jm\vartheta'} e^{jm(\pi/2 + \theta_\vartheta)} \qquad \text{(A. 11)}$$

Let us define the amplitude of plane SAW as S, where Poyinting vector of SAW is $\Pi = SS^*/2$ by the definition of S. Unitary amplitude SAW propagating in z-direction is coupled to electric potential of amplitude Φ_z, while propagating in direction ϑ is coupled to potential Φ_ϑ. Taking this into account one obtains the dependence of scattered SAW far-field on the the angle ϑ as follows

$$S(\vartheta) = \Phi(\vartheta)[\Phi_z/\Phi_{\theta_s}] \qquad \text{(A. 12)}$$

Appendix B

Let us consider an elliptic disk having main axes R/α and αR. The disk orientation in the coordinate system x, z is described by rotation angle θ_0. The disk is transformed into a circle of unitary radius on the (ξ, ζ) plane, where new cartesian coordinate system ξ, ζ is defined by

$$z/R = (\zeta/\alpha)(1 + \alpha^4 \mathrm{tg}^2\theta_0)^{1/2}\cos\theta_0$$
$$x/R = [\alpha\xi - \zeta(1 - \alpha^4)\sin\theta_0]/\cos\theta_0 \qquad \text{(B. 1)}$$

(the new system is chosen in such a way that ζ–axis is directed along z–axis, it means that the incident wave propagates along $-\zeta$–axis in new coordinate system).

Consider a wave propagating in the direction that is ϑ' rotated with respect to ξ in the new coordinate system, and the wave-number of the wave in new coordinate system is k'. In old coordinate system this wave correspond to (that is, it is transformed into) the wave with wave-number k, and its propagation direction is rotated from x–axis with angle ϑ, where

$$\mathrm{tg}\,\vartheta = \frac{(1 - \alpha^4)\mathrm{tg}\theta_0 + (1 + \mathrm{tg}^2\theta_0)\alpha^2 \mathrm{tg}\,\vartheta'}{1 + \alpha^4 \mathrm{tg}^2\theta_0}$$
$$k = sk' \qquad \text{(B. 2)}$$
$$s = \frac{1}{R}\left(\frac{(1 + \alpha^4 \mathrm{tg}^2\theta_0)}{\alpha^2(1 + \mathrm{tg}^2\theta_0)\cos^2\vartheta'}(1 + \mathrm{tg}^2\vartheta) \right)^{1/2}$$

Note also, that the point described in polar coordinates by r' and ϑ' in the new system corresponds to point described in polar coordinates by r and ϑ in old system, where

$$r = r'/s \tag{B. 3}$$

On the strength of the relation (3) the amplitude of electric potential resulting from the wave of surface charge fulfils

$$\frac{\Phi}{\Delta D_\perp} = \frac{1}{\varepsilon_e(\vartheta) s k'} \frac{(sk')^2 - k_0^2}{(sk')^2 - k_v^2} = \frac{1}{k'[s\varepsilon_e(\vartheta)]} \frac{k'^2 - (k_0/s)^2}{k'^2 - (k_v/s)^2} \tag{B. 4}$$

As we see, in the coordinate system (ξ, ζ) we obtain similar relation as in the original system (3), but with $\varepsilon_e'(\vartheta') = s\varepsilon_e(\vartheta)$, $k'(\vartheta') = k_0(\vartheta)/s$, $k_v'(\vartheta') = k_v(\vartheta)/s$ with $\vartheta = \vartheta(\vartheta')$, instead of ε_e, k_0, k_v.

The relation (36) gives the scattered potential amplitude. In the transformed coordinate system where the disk is a circular one with unitary radius. To transform the angular dependent scattered potential $\Phi(\vartheta)$ into the original system of coordinates one should take into account the relations (B.1). To apply it we need to denote polar coordinates of the same point in the old system of coordinates as r and θ, while polar coordinates in the new system (that is in the system applied in (36)) as r' and θ'. With these denotations the far-field potential wave is

$$\Phi(\theta) = \Phi(\theta')(r'/r)^{1/2} \tag{B.5}$$

where $\theta = \theta(\theta')$ and $\sqrt{(r'/r)}$ term appears above as a result of the dependence of g^A on r (θ and ϑ from (B.2) are different angles!).

It is worth to note that the scattered far-field amplitude can be also calculated directly in the original system of coordinates, with applying suitable asymptotic Green's function and charge distribution expressed in the original coordinates. The evaluation of the integral (10) however, needs integral variable transformation leading to integration over a circle. Both approaches give the same results.

Appendix C

As known, it is for integer k

$$J_{k+1/2}(z) = z^{-1/2} \sum_p \left(\frac{a_p^{(1)}}{z^p} \cos(z) + \frac{a_p^{(2)}}{z^p} \sin(z) \right)$$

where $a_p^{(1)}$ and $a_p^{(2)}$ can be found elsewhere [16], and summation after $p \geq 0$ takes place in finite limits. The above allows to rewrite (21) in form (for $l \neq 0$)

$$c_1 = (\pi/2)^2 (\operatorname{sign} m)^m \left(\sum \frac{{}^1a_p^{(m,n)}}{(\pi l/2)^p} \cos^2(\pi l/2) + \sum \frac{{}^2a_p^{(m,n)}}{(\pi l/2)^p} \sin^2(\pi l/2) + \right.$$
$$\left. + \sum \frac{{}^3a_p^{(m,n)}}{(\pi l/2)^p} \cos(\pi l/2) \sin(\pi l/2) \right) \tag{C. 1}$$

which can be further transformed into $(\cos(\pi l) = (-1)^l)$

$$c_1 = \pi(\operatorname{sign} m)^m \left(\sum_{p=P_1(2)}^{P_2} \frac{a_p^{(m,n)}}{(\pi l)^p} \cos(\pi l) + \sum_{p=P_3(2)}^{P_4} \frac{b_p^{(m,n)}}{(\pi l)^p} + \sum_{p=P_5(2)}^{P_6} \frac{d_p^{(m,n)}}{(\pi l)^p} \sin(\pi l) \right) \tag{C. 2}$$

The coefficients a, b and d can be easily calculated numerically, it is also easy to check that the following Property I takes place

PROPERTY I

a) $b_p^{(0,n)} b_p^{(l,n)} = 0$

what means, that there is not the second component in brackets in (C.2) for $m = 0$ or $m = 1$,

b) in (C.2) the summation after p is **step 2** and takes place in the following limits (m and n have the same parity)

$P_1 = 2$ for m even or 1 for m odd,

$P_2 = n$,

$P_3 = 2$ for n even or 1 for n odd,

$P_4 = |m|$,

$P_5 = 1$ for m even or 2 for m odd,

$P_6 = n + 1$,

c) in (C.2) the number of components of $(+1)^l/l^p$ kind is $|m/2|$ (integer part of the product for m odd).

The polynomial (24) can be written as a combination of Tchebyshev polynomials of the lower orders as follows [16]

$$T_n^{(m)} = T_n - \sum_{k(2)}^{|m|-2} t_k^{(m,n)} T_k \tag{C. 3}$$

where t_k are easy to find and where summation after k starts from 0 for m even or 1 for m odd, step 2, to $|m| - 2$.

The following Property II takes place for every m and $n \geq |m|$

PROPERTY II

$$b_p^{(m,n)} - \sum_{k}^{|m|-2} t_k^{(m,n)} b_p^{(m,n)} = 0 \tag{C. 4}$$

The formal proof of (C.4) is expected very tedious, but it is very easy to check it numerically. All numbers appearing in (C.4) are integers so that the numerical check of (C.4) may be considered exact and sufficient for our purpose in the paper.

Now consider charge distribution in the form of (24). On the strength of (C.4) we obtain the representation (26) for potential under the disk, where components like $(+1)^l/l^p$ does not appear and

Table 1. Coefficients $\alpha_p^{(m,n)}$ and $\gamma_1^{(m,n)}$ for some m and $n \geq m$ in following rows, in subsequent columns α_p are arranged with growing p except the cases of even m, where in the first column γ_1 is presented.

		γ_1 even)	α_2 (m even)	α_4	...	
m	n	a_1 (m odd)	α_3 (m odd)	α_5	...	
0	2	1	2			
	4	1	8	-72		
	6	1	18	-912	7200	
	8	1	32	-5280	192000	-1411200
1	1	-1				
	3	-1	12			
	5	-1	84	-720		
	7	-1	312	-13200	100800	
	9	-1	840	-104880	3528000	-25401600
2	2	-2	-6			
	4	0	-8	120		
	6	-2	-22	1200	-10080,	
	8	0	-32	6240	-241920	1814400
3	3	4	-60			
	5	-4	-100	1680		
	7	8	-472	21840	-181440	
	9	-8	-936	146160	-5382720	39916800
4	4	8	80	840		
	6	-16	-128	-1680	30240	
	8	32	320	-11424	483840	-3991680
5	5	-16	1680	-15120		
	7	48	-3696	-35280	665280	
	9	-112	11184	-315504	12640320	-103783680
6	6	-32	-672	40230	-332640	
	8	128	2560	-112896	-887040	17297280

$$\alpha_0^{(m,n)} = (\operatorname{sign} m)^m \left(a_p^{(m,n)} - \sum_k t_k^{(m,n)} a_p^{(m,k)} \right) \tag{C.5}$$

Table I presents values of α for some indices m, n, and p. The calculation were performed in double precision (18 decimal digits). Note that the values presented in Table I are integer numbers so that their values can be considered as exact ones.

Appendix D

Consider an expression $1/(n^2 - \varepsilon^2)$ for $\varepsilon < 1$ firstly. It can be expanded into a Taylor series as follows

$$\frac{1}{n^2 - \varepsilon^2} = \frac{1}{n^2} + \frac{\varepsilon^2}{n^4} + \ldots + \frac{\varepsilon^{2N}}{n^{2N}} \left(\frac{1}{n^2} + \frac{\varepsilon^2}{n^4} + \ldots \right) \tag{D. 1}$$

The Lagrange interpolation formula applied to (D.1) for $n = 1, 2, \ldots, N$ yields (below, there is strict equality for n in the above limits, a_n is given in rel. 3.1.1 of [17], for instance)

$$\frac{1}{n^2 - \varepsilon^2} = \frac{a_1}{n^2} + \frac{a_2}{n^4} + \ldots + \frac{a_{2N}}{n^{2N}}; \quad n = 1, 2, \ldots, N \tag{D. 2}$$

By comparison of (D.1) and (D.2) we see that applying $a_1 = 1$, $a_2 = \varepsilon^2, \ldots, a_N = \varepsilon^{2(N-1)}$ we admit an error to (D.2) of an order of $\varepsilon^{2N}/(1 - \varepsilon^2)$ thus vanishing for $N \to \infty$. It means that $a_1 \to 1$ for $N \to \infty$, similarly a_2 becomes constant dependent on ε etc. This reflects fact that $(n^2 - \varepsilon^2)^{-1}$ is close to n^{-2} for $n > N \to \infty$.

The above is difficult to prove for $\varepsilon > 1$ so we show it numerically in Table II below for N between 4 and 10 and for some ε (only a_1 is shown in the Table)

Table 2. First coefficient a_1 of Lagrange interpolation (D.2)

$\varepsilon^2 \backslash N$	4	5	6	7	8	9	10
.25	.99999	1.	1.	1.	1.	1.	1.
.9	.98270	1.0006	.99998	1.	1.	1.	1.
2.5	1.1978	.97802	1.0016	.99991	1.	1.	1.
3.9	19.927	-1.389	1.2903	.97490	1.0016	.99992	1.
9.5	54.608	-31.86	12.779	-1.833	1.4938	.93439	1.0069

Most important conclusion is that at least the leading term of Lagrange interpolation (D.2), that is the term a_1/n^2, became $1/n^2$ for large N. So applying (D.2) beyond its validity area, that is for all $n = 1, 2, \ldots, N, \ldots\infty$, we admit error of an order of $0(1/N^2)$.

References

[1] J.J. BOWMAN, T.B.A. SENIOR, P.L.E. USLENGHL, *Electromagnetic and acoustic scattering by simple shapes*, Nord-Holland, Amsterdam 1969.

[2] W.H. EGGLMAN, *Higher-order evaluation of electromagnetic diffraction by circular disks*, IRE Trans., **MIT–9**, 5, 408–419 (1961), **81**, 6, 1677–1682 (1987).

[3] F.J. SABINA, *General formulas for low-frequency acoustic scattering by soft body or disk*, JASA, **81**, 6, 1677–1682 (1987).

[4] B.A. AULD, *Acoustic fields and waves in solids*, A. Wiley Interscience Publ., NY.1973.

[5] K.A. INGEBRIGSTEN, *Surface waves in piezoelectrics*, J. Appl. Phys., **40**, 7, 2681–2686 (1969).

[6] R.F. MILSOM, N.H.C. REILLY, M. REDWOOD, *Analysis of generation and detection of surface and bulk acoustic waves by interdigital transducers*, IEEE Trans., **SU-24**, 3, 147–166 (1977).

[7] E. DANICKI, *Propagation of transverse surface acoustic waves in rotated Y-cut quartz substrates under heavy periodic metal electrodes*, IEEE Trans. **SU-30**, 5, 304–314 (1983).

[8] E. DANICKI, *Influence of bulk wave generation on SAW filter performance*, J. Tech. Phys., **21**, 3, 405–420 (1980).

[9] A.P. PRUDNIKOV, J.A. MARICHEV, *Integrals and series*, (in Russian), Nauka, Moscow 1986, v. 2.

[10] F. OBERHETTINGER, W. MAGNUS, *Adwendung der Elliptischen Functionen in Physik und Technik*, Springer Verlag, Berlin 1949.

[11] E. DANICKI, *Green's function for anisotropic dielectric halfspace,* IEEE Trans. **UFFC-35**, 5, 643 (1988).

[12] J.B. FELSEN, N. MARCUVITZ, *Radiation and scattering of waves*, Prentice Hall Englewood Cliff 1973.

[13] E. DIEULESAINT, D. ROYER, *Ondes elastiques dans les solides*, Masson, Paris 1974.

[14] A.A. MARDUDIN, *Surface acoustic waves on real surfaces,* ISSWAS'66 Proc., v.3, 22–62, Novosibirsk 1986.

[15] E. DANICKI, *Theory of Williamson's SAW probe* (in Polish) OSA'88 Proc. Warszawa 1988, 251–254.

[16] H. BATEMAN, A. ERDELY, *Higher transcendential functions*, McGraw-Hill 1953 v.2.

[17] W.H. PRESS, B.P. FLANNERY, S.A. TEUKOLSKY, N.T. VETTERLING, *Numerical recipes*, Cambridge Univ. Press 1986.

[18] J. BOERSMA, E. DANICKI, *On the solution of an integral equation arising in potential problem for circular and elliptic disk*, submitted for publication in SIAM J. Appl. Math., (1992).

Received February 5, 1991